nature energy

Article

https://doi.org/10.1038/s41560-023-01240-9

In situ monitoring redox processes in energy storage using UV–Vis spectroscopy

In the format provided by the authors and unedited

Supplementary Information

Table of Contents

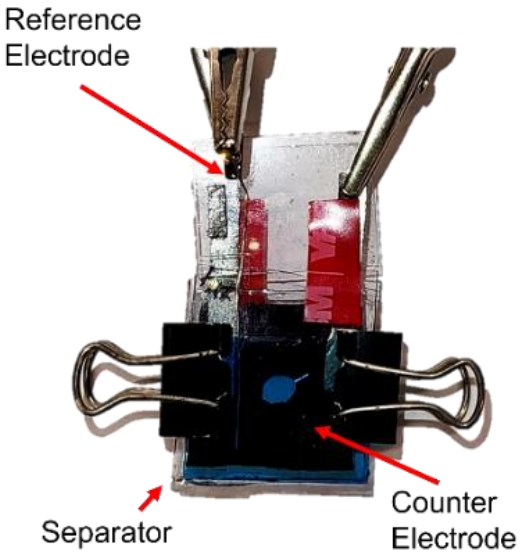

Supplementary Figure 1. ***In situ*** **UV-Vis three-electrode cell used in this study.**

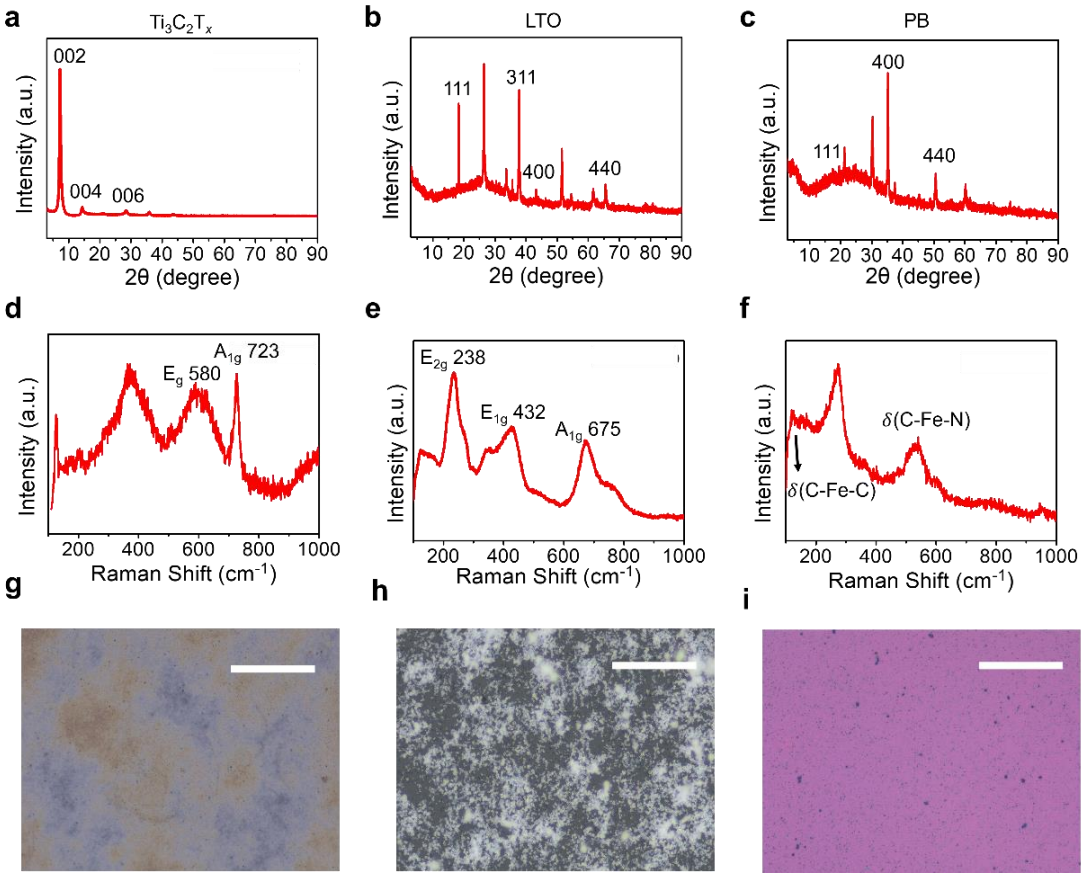

Supplementary Figure 2. Physical characterization of $Ti_3C_2T_x$,[1,2] lithium titanate (LTO),[3] and Prussian blue (PB)[4] thin films. a, b, c, XRD patterns and **d, e, f,** Raman spectra. **g, h, i,** Optical images of the corresponding films. The scale bar is 50 μm. The plane roughness values of the corresponding films are 32±5 nm, 389±21 nm, and 25±3 nm, respectively.

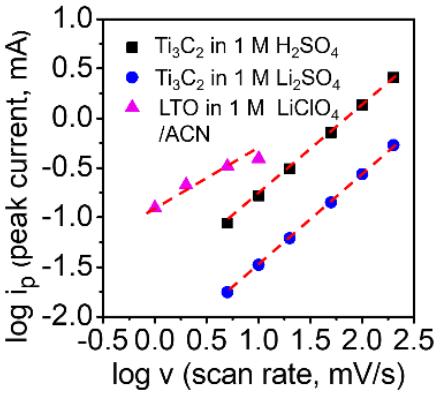

Supplementary Figure 3. **Determination of *b* value (slope) for logarithm of anodic peak current (i_p) versus the logarithm of the scan rate (v) of these three systems.** For $Ti_3C_2T_x$ in 1 M Li_2SO_4 (blue spheres, v = 5, 10, 20, 50, 100 mV/s), b = 0.916, R^2 = 0.999. For $Ti_3C_2T_x$ in 1 M H_2SO_4 (black squares, v = 5, 10, 20, 50, 100 mV/s), b = 0.921, R^2 = 0.999. For LTO in 1 M $LiClO_4$/acetonitrile (ACN) (purple triangles, v = 0.5, 1, 2, 5, 10 mV/s), b = 0.499, R^2 = 0.941.

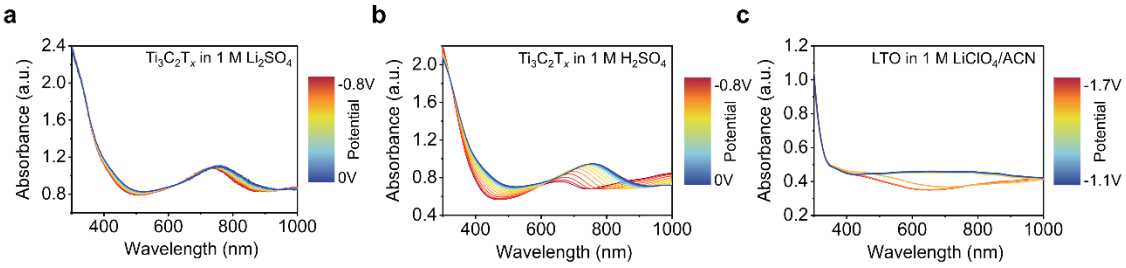

Supplementary Figure 4. ***In situ*** **UV-Vis absorption spectra in the anodic cycle. a,** $Ti_3C_2T_x$ in 1 M Li_2SO_4, **b,** $Ti_3C_2T_x$ in 1 M H_2SO_4, and **c,** LTO in 1 M $LiClO_4$/acetonitrile (ACN) in anodic cycle.

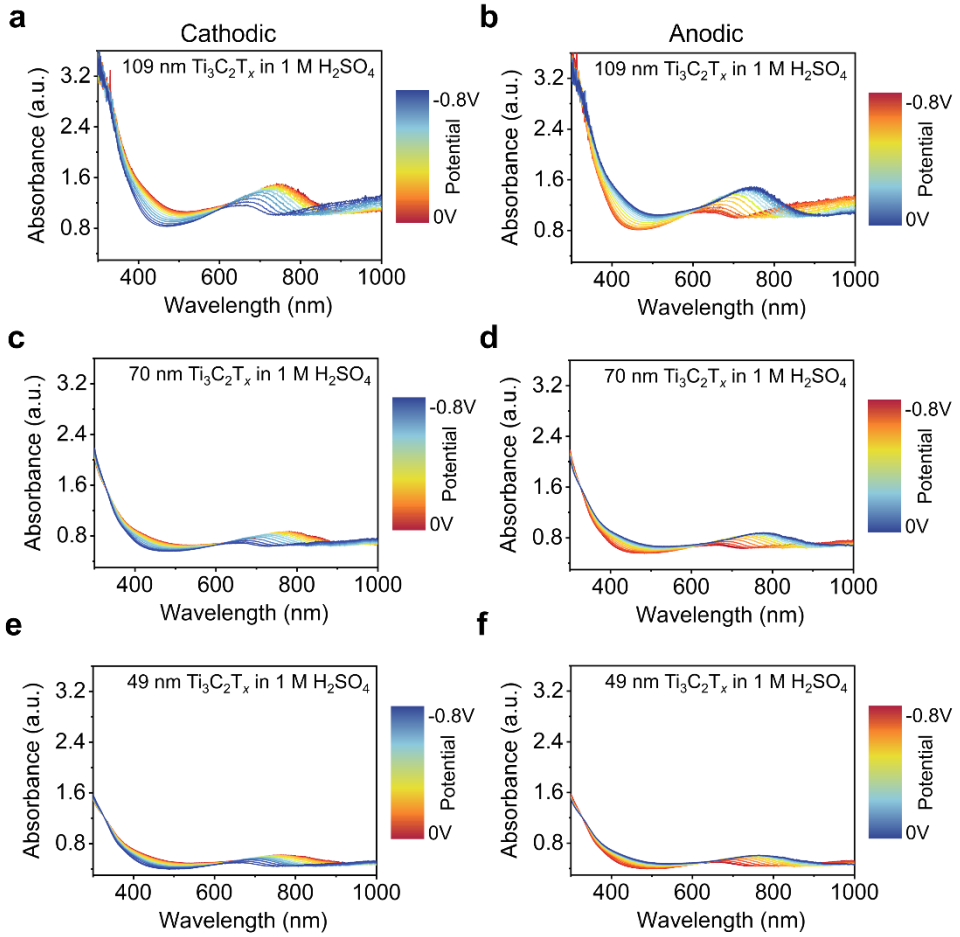

Supplementary Figure 5. ***In situ*** **UV-Vis absorption spectra of $Ti_3C_2T_x$ of different thicknesses in 1 M H_2SO_4. a, b,** 109 nm, **c, d,** 70 nm, **e, f,** 49 nm. **a, c, e** Cathodic cycles and **b, d, f** Anodic cycles.

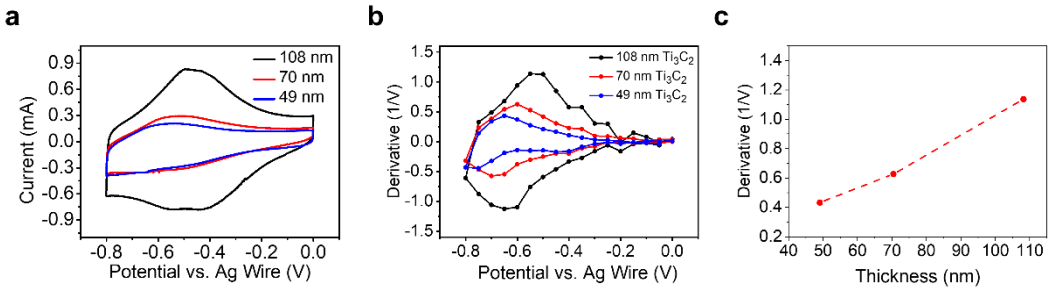

Supplementary Figure 6. **Thickness-dependent *in situ* UV-Vis data from $Ti_3C_2T_x$ in 1 M H_2SO_4. a,** Typical cyclic voltammograms (CVs) of $Ti_3C_2T_x$ in 1 M H_2SO_4 with different thickness (108 nm, 70 nm, 49 nm). **b,** Absorbance derivative (obtained with MUSCA method) versus potential of $Ti_3C_2T_x$ with different thickness. **c,** Plot of the largest absorbance derivative values versus thickness.

Supplementary Note 1

To evaluate the impact of electrode coating thickness first, we compared the derivatives of $Ti_3C_2T_x$ electrodes with three different thicknesses in 1 M H_2SO_4. All the samples

with the thickness of 49 nm, 70 nm and 109 nm show the same trend in the peak shift from ~780 nm to ~620 nm. However, the absorbance change of the plasmonic peak is thickness dependent as shown in Supplementary Figure 6b. The maximum value of the absorbance derivative increases almost linearly with the electrode thickness (Supplementary Figure 6c). Hence, the effect of electrode thickness was subtracted to normalize the derivative value in different systems.

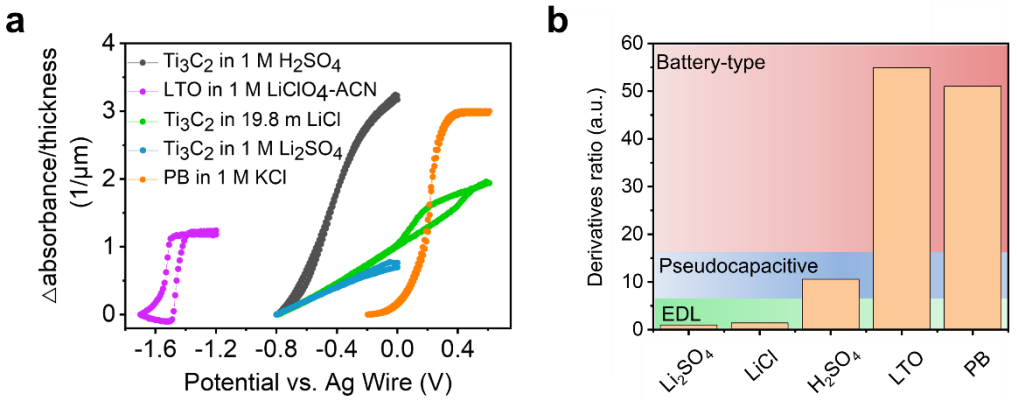

Supplementary Figure 7. The distinction of charge storage mechanisms with the slope of relative absorbance change and normalized derivative. a, Relative absorbance change in the UV-Vis absorption spectra at the signature wavelength for lithium titanate (LTO) in 1 M $LiClO_4$/acetonitrile (ACN), $Ti_3C_2T_x$ in 1 M H_2SO_4, $Ti_3C_2T_x$ in 1 M Li_2SO_4, $Ti_3C_2T_x$ in 19.8 m LiCl and Prussian Blue (PB) in 1 M KCl. **b,** Distinguishing electrical double-layer, pseudocapacitive, and battery-type charge storage mechanisms by comparing derivative ratios for $Ti_3C_2T_x$ in 1 M Li_2SO_4 (Li_2SO_4), $Ti_3C_2T_x$ in 19.8 m LiCl (LiCl and LiCl peak, which means the derivative at CV peaks), $Ti_3C_2T_x$ in 1 M H_2SO_4 (H_2SO_4), LTO in 1 M $LiClO_4$/ACN (LTO), PB in 1 M KCl (PB).

Supplementary Note 2

$$Relative\ absorbance\ change = \frac{A_{neg} - A_x}{l} \quad (1)$$

where A_x represents UV-Vis absorbance of signature wavelength at x V, A_{neg} represents UV-Vis absorbance of signature wavelength at the most negative potential, and l represents film thickness.

The plots show relative absorbance change at the signature wavelength. The $Ti_3C_2T_x$ films in 1 M Li_2SO_4 and $Ti_3C_2T_x$ in 19.8 m LiCl systems show gradual decreases of the UV-Vis absorbance with increasing potential, which indicates that the double layer capacitance contributes little to the change of Ti oxidation state. LTO films in 1 M $LiClO_4$/ACN and PB in 1 M KCl have abrupt decreases of the UV-Vis absorbance with increased potential at the peak position of CVs, which indicates the Faradaic process contributes to the oxidation state change of the battery materials and results in a steep slope. The $Ti_3C_2T_x$ in 1 M H_2SO_4 system shows median slope within the range of the surface redox peaks (between -0.4 V and -0.8 V).

The derivatives ratio in Supplementary Figure 7b is calculated using the following equation, where the data were collected with the MUSCA method:

$$Derivatives\ ratio = \overline{D_{total}}/D_{EDL} \quad (2)$$

where $\overline{D_{total}}$ stands for the total average normalized derivative of the selected peak region (i.e., 0.3 to 0.4 V for $Ti_3C_2T_x$ in 19.8 m LiCl and -0.8 to -0.4 V for $Ti_3C_2T_x$ in 1 M H_2SO_4) and D_{EDL} represents the normalized derivative at the EDL region.

$$Normalized\ derivative_x = \frac{A_x - A_{x-\Delta E}}{\Delta E \cdot l} \quad (3)$$

Where A_x is the signature absorbance at x V, ΔE is the potential difference between each step (0.05 V in this case), and v is the scan rate.

Supplementary Note 3

The charges in Figures 3a, 3b, and 3c were calculated from the MUSCA profiles in Supplementary Figure 13 and expressed as:

$$Q_m = \sum_{E_{pos}}^{x=m} \int_0^{150} i_x dt \quad (4)$$

Q_m represents charge at m V. E_{pos} represents the most positive potential (0 V for $Ti_3C_2T_x$ in 1 M H_2SO_4 and Li_2SO_4, -1.2 V for LTO in 1 M $LiClO_4$/ACN). I_x represents the current at x V during MUSCA measurement. 150 represents 150 s step time at each potential during MUSCA measurement. From *in situ* UV-Vis spectra, we know the absorbance intensities at m V and after calculating the charge at m V we plot them as shown in Supplementary Figure 9 and Figures 3a 3b, and 3c. k is the slope of these plots determined by linear fitting, and a larger k value indicates the redox reactions as discussed in manuscript.

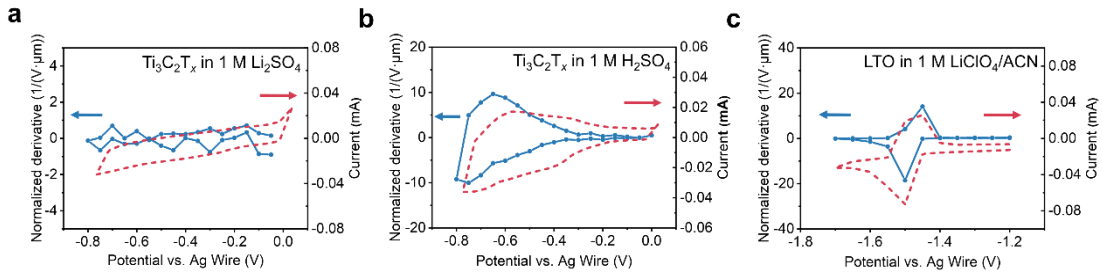

Supplementary Figure 8. Normalized derivative and electrochemical cyclic voltammograms with MUSCA method (1 mV/s). a, $Ti_3C_2T_x$ in 1 M Li_2SO_4, **b,** $Ti_3C_2T_x$ in 1 M H_2SO_4, **c,** Lithium titanate (LTO) in 1 M $LiClO_4$/acetonitrile (ACN).

Supplementary Note 4

The method of calculating the absorbance derivative is based on the combination of Faraday's law and Beer's law. We can assign the total amount of electrode material as τ^0 and the extinction coefficients of a material in oxidized and reduced states as ε_{ox} and ε_{re}. During the anodic cycle, a certain amount of material is oxidized, which can be described by Faraday's law of electrolysis:

$$Q = nF\tau_{ox} \quad (5)$$

where Q is the charge consumed in the electrochemical reaction, F is the Faraday constant, n is the number of electrons participating in the electrochemical reaction, and τ_{ox} is the molar amount of the oxidized material. The absorbance, according to Beer's, law is:

$$A = l(\varepsilon_{ox} \times \frac{\tau_{ox}}{\tau^0} + \varepsilon_{re} \times \frac{\tau^0 - \tau_{ox}}{\tau^0}) = l\left((\varepsilon_{ox} - \varepsilon_{re})\frac{\tau_{ox}}{\tau^0} + \varepsilon_{re}\right) \quad (6)$$

where l is the thickness of the electrode material. The variation of absorbance, ΔA, accompanied by the potential change is:

$$\Delta A = l(\varepsilon_{ox} - \varepsilon_{re}) \times \frac{\Delta\tau_{ox}}{\tau^0} = l(\varepsilon_{ox} - \varepsilon_{re}) \times \frac{\Delta Q}{\tau^0 nF} \quad (7)$$

where $\Delta\tau_{ox}$ is the change of oxidation states and ΔQ is the change of stored charge. Similarly, the incremental change of absorbance with respective to time, Δt, can be:

$$\Delta A/_{\Delta t} \propto \Delta Q/_{\Delta t} = I \quad (8)$$

where I is current passed through the system during Δt. The derivation shows that the absorbance is directly related to the charge and the variation of absorbance is proportional to the current. This agrees with a previous study.[5] This derivation provides a theoretical foundation for the UV-Vis CVs and explains why they agree well with the electrochemical experimental data.

The MUSCA method derived normalized derivative plots in Supplementary Figure 8 show a good correlation between normalized derivative at x V, D_x, and electrochemical CVs:

$$Normalized\ derivative_x = \frac{A_x - A_{x-\Delta E}}{\Delta E \cdot l} = \frac{A_x - A_{x-\Delta E}}{\Delta t \cdot v \cdot l} \propto i \quad (9)$$

where ΔE is the potential difference between each step (0.05 V in this case) and v is scan rate. Because scan rate in a cyclic voltammetry experiment is constant, the normalized derivative is proportional to current.

Supplementary Note 5

For the LTO electrode in 1 M $LiClO_4$/ACN, there are three typical processes in the cathodic cycle in Figure 3c and Supplementary Figure 9. However, it is difficult to distinguish three stages in the anodic cycle; the reason comes from the low Coulombic efficiency of this battery-type device (as seen in Figure 2c), where the current is still negative when the potential begins increasing from -1.7 V. Despite this, k_{4c2}, which represents the potential range where redox reaction happens, is still larger than k_{4c1} and k_{4c3}, which represent non-Faradaic ion insertion and parasitic reactions, respectively. Similar results were also obtained using cyclic voltammetry (CV) method. Supplementary Figure 9 shows a good linearity between the charge and the relative absorbance change, which demonstrates that one can perform further derivative analysis, as discussed in the "Coupling between charge transfer and UV-Vis spectral changes" section of the main manuscript.

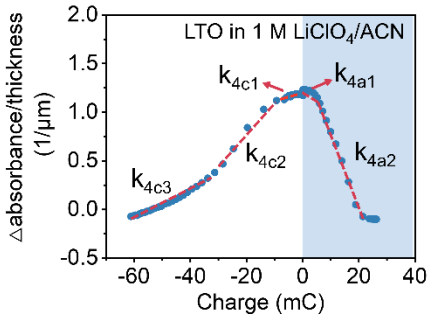

Supplementary Figure 9. **Absorbance change versus charge and linear data fitting for lithium titanate (LTO) in 1 M $LiClO_4$/ acetonitrile (ACN) with the CV method**. The blue shade means the anodic cycle. k_c is the cathodic slope and k_a is the anodic slope, respectively. The linear fitting results are shown in Supplementary Table 1.

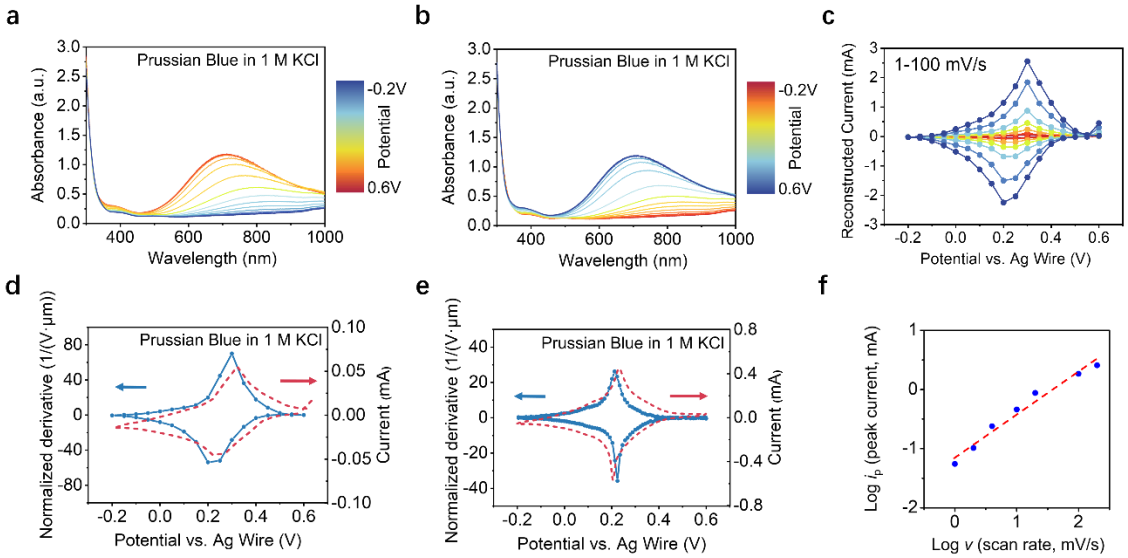

Supplementary Figure 10. ***In situ*** **UV-Vis characterization of Prussian Blue (PB) in 1 M KCl. a, b,** *in situ* absorption spectra of Prussian blue in 1 M KCl from 300 nm to 1000 nm in cathodic and anodic cycles, respectively. **c,** Reconstructed voltammograms obtained from MUSCA data. **d,** Normalized derivative at 700 nm and reconstructed voltammograms at 1 mV/s from the MUSCA method. **e,** Normalized derivative at 700 nm and cyclic voltammograms at 10 mV/s from the CV method. **f,** Determination of b value (slope) from the logarithm of anodic peak current (i_p) versus the logarithm of the scan rate (v) from **c**. $b = 0.719$, $R^2 = 0.966$.

Supplementary Note 6

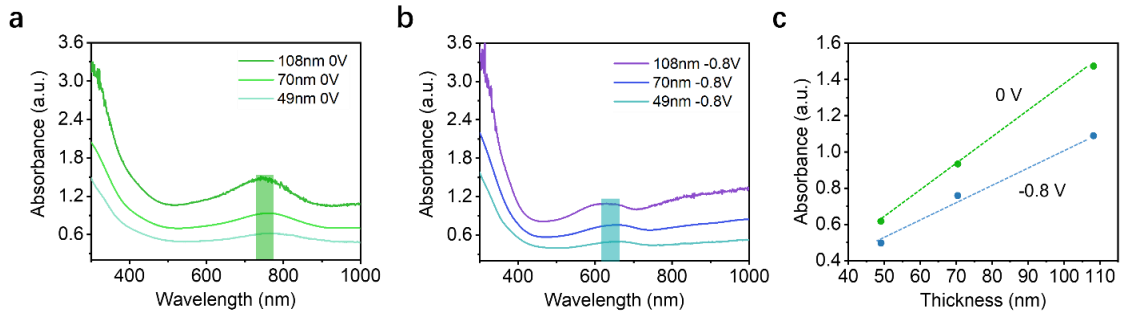

Supplementary Figure 11. Determining the extinction coefficients of $Ti_3C_2T_x$ in the oxidized state (0 V) and the reduced state (-0.8 V) in 1 M H_2SO_4. a, b, *in situ* UV-Vis absorption spectra of the $Ti_3C_2T_x$ films having three different thicknesses at 0 V and -0.8 V. **c,** Plot of the absorbance at the peak position versus thickness at 0 V and -0.8 V.

As shown in Supplementary Figure 11, using films with different thicknesses cycled in 1 M H_2SO_4, one can calculate the extinction coefficients of $Ti_3C_2T_x$ in the oxidized state (ε_{ox} at 0 V) and the reduced state (ε_{re} at -0.8 V) for this specific system:

$$\varepsilon = \frac{A}{l} \tag{10}$$

From the slopes of Supplementary Figure 11, we get ε_{ox} = 0.01447 1/nm and ε_{re} = 0.00987 1/nm. For $Ti_3C_2T_x$ in 1 M H_2SO_4, if we take the absorbance change and charge (MUSCA method) during the cathodic cycle, then substitute these values to equation (5):

$$-0.17474 = 70\ nm \times (0.01447 - 0.00987)(1/nm) \times \frac{-0.2714\ mA \times 50\ s}{96485\ \frac{C}{mol}} \times \frac{1}{n} \times \frac{1}{0.120\ mg \Big/ 204.65 \frac{g}{mol}}$$

The mass of the electrode materials was 0.120 mg. The molar mass of $Ti_3C_2T_x$ (204.65 g/mol) assumes the $Ti_3C_2O_{0.300}OH_{0.614}F_{1.016}Cl_{0.070}$ composition, which was determined in our recent secondary-ion mass spectroscopy study.[6] Then the electron transfer number obtained from UV-Vis is n = 0.442 per $Ti_3C_2T_x$ (0.147 electrons per Ti atom), close to the 0.134 electrons per Ti atom obtained from *in situ* XAS.[7]

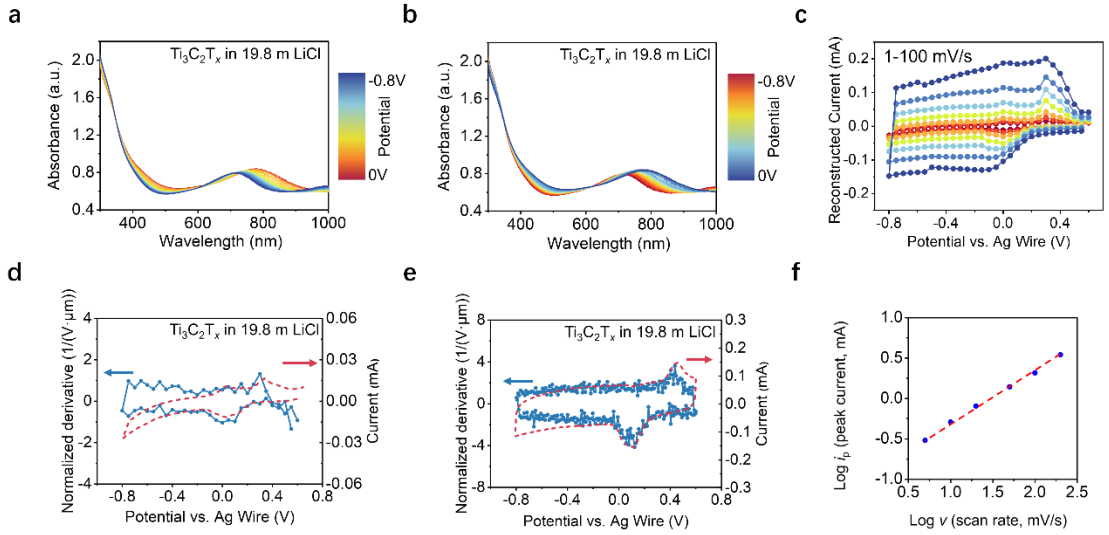

Supplementary Figure 12. ***In situ*** **UV-Vis characterization of $Ti_3C_2T_x$ in 19.8 m LiCl. a**, **b**, *in situ* absorption spectra of $Ti_3C_2T_x$ in 19.8 m LiCl from 300 nm to 1000 nm in cathodic and anodic cycles, respectively. **c**, Reconstructed voltammograms obtained from MUSCA data. **d**, Normalized derivative of plasmonic peak and reconstructed voltammograms at 1 mV/s from the MUSCA method. **e**, Normalized derivative at 450 nm and cyclic voltammograms at 10 mV/s from the CV method. **f**, Determination of *b* value (slope) for logarithm of anodic peak current (i_p) versus the logarithm of the scan rate (v) from **c**. $b = 0.645$, $R^2 = 0.998$.

Supplementary Note 7

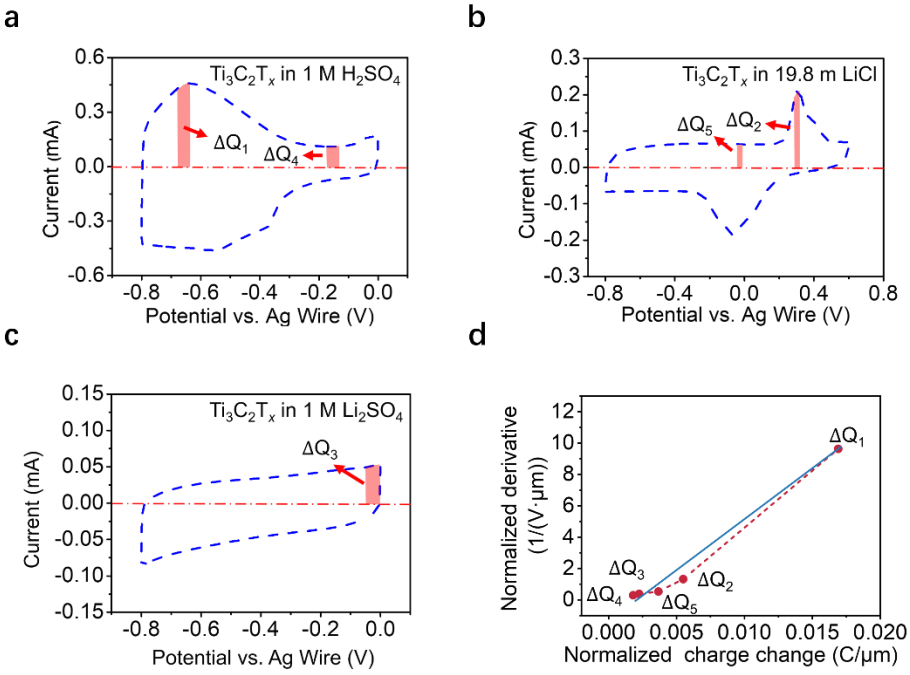

Supplementary Figure 13. **Relationship between charge and derivative within the**

same potential window. a, Charge in the redox-peak (-0.60 V to -0.65 V) and double-layer (-0.2 V to -0.15 V) potentials windows for $Ti_3C_2T_x$ in 1 M H_2SO_4. The CV is the same data as in Supplementary Figure 8b. **b,** Charge in the peaks (0.25 V to 0.3 V) and double-layer (-0.1 V to -0.05 V) potential windows of $Ti_3C_2T_x$ in 19.8 m LiCl. The CV is the same as in Supplementary Fig. 11d. **c,** Charge in the double-layer potential window (0.4 V to 0.45 V) of $Ti_3C_2T_x$ in 1 M Li_2SO_4. The CV is the same as in Supplementary Fig. 8a. **d,** Normalized derivative as a function of normalized charge change.

The normalized charge change, ΔQ_x, are calculated as below:

$$\Delta Q_x = \frac{i_x \times 2.5\ s}{l} \tag{11}$$

The ΔQ_1, ΔQ_4, are calculated at -0.6 V and -0.15 V for $Ti_3C_2T_x$ in 1 M H_2SO_4. ΔQ_2, ΔQ_5 are at 0 V and 0.35 V for $Ti_3C_2T_x$ in 19.8 m LiCl. ΔQ_3 is at 0 V for $Ti_3C_2T_x$ in 1 M Li_2SO_4. In the cases of rectangular CV curves in Supplementary Figures 13a and 13b recorded in H_2SO_4 and LiCl electrolytes (ΔQ_4 and ΔQ_5), the ion insertion results in the EDL formation. The normalized derivatives are also small, and they change at an almost constant rate in these regions. For $Ti_3C_2T_x$ in 1 M H_2SO_4, the normalized derivatives (as shown in Supplementary Figure 8b) increase much more dramatically at the peak region (like ΔQ_1 region) than the current at the onset potential of the surface redox reaction, which demonstrated that surface redox reaction leads to a relatively enormous change in the UV-Vis spectra. In comparison, for $Ti_3C_2T_x$ in 19.8 m LiCl, the normalized derivatives are nearly at an identical extent at the EDL region (ΔQ_5) and the peak region (ΔQ_2).

For electrochemical systems especially pseudocapacitive systems, the total current, i_{total}, can be separated into two parts generally:

$$i_{total} = i_{EDL} + i_{redox} \tag{12}$$

where i_{EDL} represents the EDL contributed current and i_{redox} represents the redox contributed current.

Based on the relationship between i and ΔA in equation (7), equation (10) can be converted to:

$$\Delta A_{total} = \Delta A_{EDL} + \Delta A_{redox} \tag{13}$$

where ΔA_{total} represents the total normalized derivative at a certain potential, ΔA_{EDL} and ΔA_{redox} represent the EDL contributed and redox contributed normalized derivative, respectively.

Following equation (7), the normalized derivative can also be calculated as:

$$D_{total} = D_{EDL} + D_{redox} \tag{14}$$

where D_{total} represents the total normalized derivative at a certain potential, D_{EDL} and D_{redox} represent the EDL contributed and redox contributed normalized derivative.

Assuming the absorbance change contributed by EDL remains the same within the electrochemical window if the surface doesn't change significantly, we drew the red regions in Figure 5 for electrochemical and UV-Vis CVs in the manuscript. The challenge is to determine the charge storage mechanisms in the peak regions marked as the shaded areas in Figure 5. Herein, we determined the average normalized derivative

(ΔD) at the anodic peak potential for distinguishing EDL and redox mechanisms:

$$\Delta D = \overline{D_{total}} - D_{EDL} \quad (15)$$

where $\overline{D_{total}}$ stands for the total average normalized derivative of the selected peak region (i.e., 0.3 to 0.4 V for $Ti_3C_2T_x$ in 19.8 m LiCl and -0.8 to -0.4 V for $Ti_3C_2T_x$ in 1 M H_2SO_4).

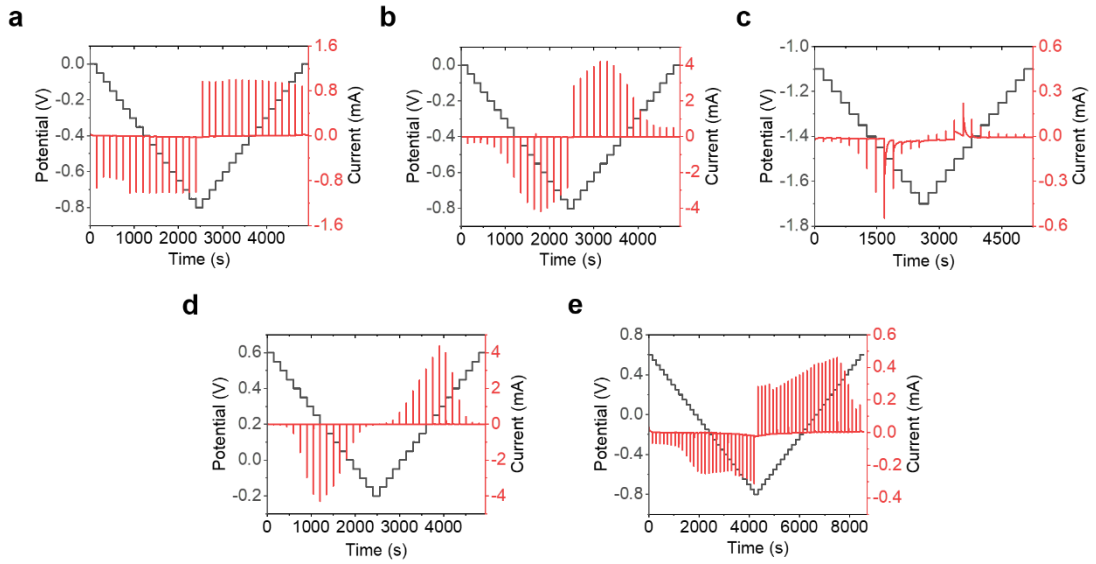

Supplementary Figure 14. **Multiple potential step chronoamperometry (MUSCA) profiles.** The black lines represent the potential vs. time and red lines represent the current vs. time. **a,** $Ti_3C_2T_x$ in 1 M Li_2SO_4, **b,** $Ti_3C_2T_x$ in 1 M H_2SO_4, **c,** lithium titanate (LTO) in 1 M $LiClO_4$/ acetonitrile (ACN), **d,** Prussian blue (PB) in 1 M KCl and **e,** $Ti_3C_2T_x$ in 19.8 m LiCl.

Supplementary Table 1. The slope and *R* value of linear fitting of normalized absorbance change versus charge of $Ti_3C_2T_x$ in 1 M Li_2SO_4, $Ti_3C_2T_x$ in 1 M H_2SO_4 and LTO in 1 M $LiClO_4$/acetonitrile (ACN). The unit of slope is 1/(mC·μm)

$Ti_3C_2T_x$ in 1 M Li_2SO_4					
Cathodic			Anodic		
	Slope	R^2		Slope	R^2
k_{1c}	0.0037	0.978	k_{1a}	-0.0040	0.965
$Ti_3C_2T_x$ in 1 M H_2SO_4					
Cathodic			Anodic		
	Slope	R^2		Slope	R^2
k_{2c1}	0.0091	0.941	k_{2a1}	-0.0098	0.966
k_{2c2}	0.1731	0.929	k_{2a2}	-0.2264	0.978
LTO in 1 M $LiClO_4$/CAN (MUSCA method)					
Cathodic			Anodic		
	Slope	R^2		Slope	R^2
k_{3c1}	-0.0012	0.957	k_{3a}	-0.1121	0.997
k_{3c2}	0.0045	0.984	/	/	/
k_{3c3}	0.0006	0.732	/	/	/
LTO in 1 M $LiClO_4$/ACN (CV method)					
Cathodic			Anodic		
	Slope	R^2		Slope	R^2
k_{4c1}	0.0012	0.918	k_{4a1}	-0.0007	0.446
k_{4c2}	0.0038	0.995	k_{4a2}	-0.0079	0.997
k_{4c3}	0.0012	0.983	/	/	/

Supplementary References

1 Sarycheva, A. & Gogotsi, Y. Raman spectroscopy analysis of the structure and surface chemistry of $Ti_3C_2T_x$ MXene. *Chem. Mater.* **32**, 3480-3488, (2020).

2 Mathis, T. S. *et al.* Modified MAX phase synthesis for environmentally stable and highly conductive Ti_3C_2 MXene. *ACS Nano* **15**, 6420-6429, (2021).

3 Liu, J., Wei, X. & Liu, X.-W. Two-dimensional wavelike spinel lithium titanate for fast lithium storage. *Sci. Rep.* **5**, 9782, (2015).

4 Saeed, S. *et al.* Understanding electrochemical cation insertion into prussian blue from electrode deformation and mass changes. *Chem. Commun.* **57**, 6744-6747, (2021).

5 Kim, Y. S., Harris, K. D., Limoges, B. & Balland, V. On the unsuspected role of multivalent metal ions on the charge storage of a metal oxide electrode in mild aqueous electrolytes. *Chem. Sci.* **10**, 8752-8763, (2019).

6 Michałowski, P. P. *et al.* Oxycarbide MXenes and MAX phases identification using monoatomic layer-by-layer analysis with ultralow-energy secondary-ion mass spectrometry. *Nat. Nanotech.* **17**, 1192-1197, (2022).

7 Shao, H. *et al.* Unraveling the charge storage mechanism of $Ti_3C_2T_x$ MXene electrode in acidic electrolyte. *ACS Energy Lett.* **5**, 2873-2880, (2020).